

Unrecognizable Yet Identifiable: Image Distortion with Preserved Embeddings

Dmytro Zakharov^a, Oleksandr Kuznetsov^{b,*}, Emanuele Frontoni^b

^a*Department of Applied Mathematics, V.N. Karazin Kharkiv National University, 4 Svobody Sq., Kharkiv, 61022, Ukraine*

^b*Department of Political Sciences, Communication and International Relations, University of Macerata, Via Crescimbeni, 30/32, Macerata, 62100, Italy*

Abstract

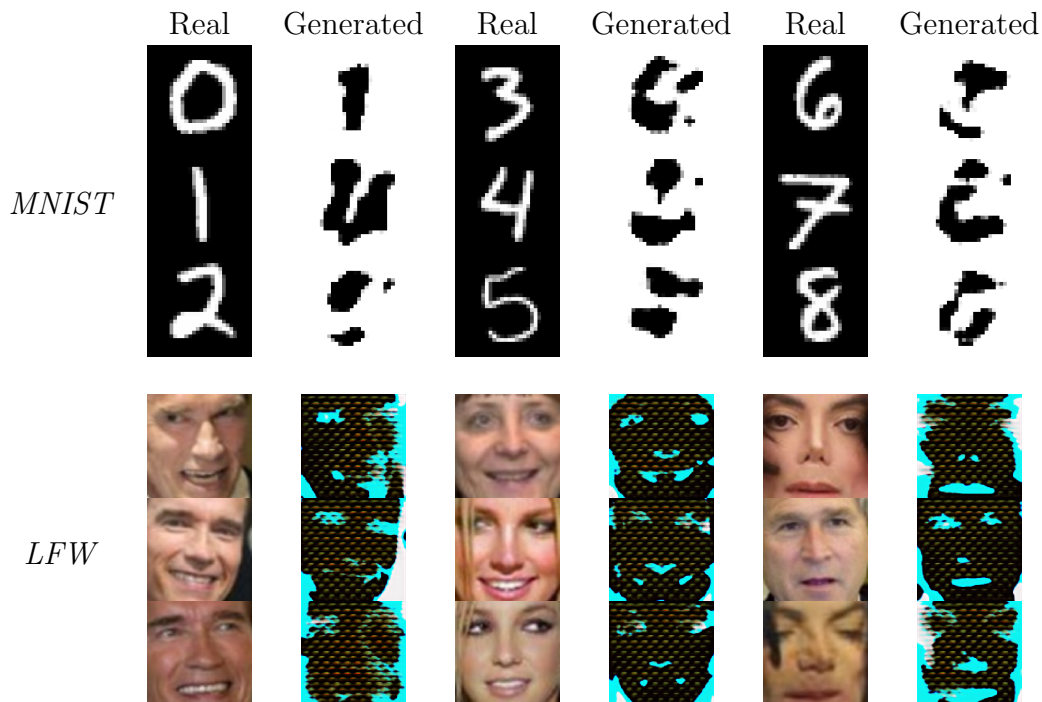
In the realm of security applications, biometric authentication systems play a crucial role, yet one often encounters challenges concerning privacy and security while developing one. One of the most fundamental challenges lies in avoiding storing biometrics directly in the storage but still achieving decently high accuracy. Addressing this issue, we contribute to both artificial intelligence and engineering fields. We introduce an innovative image distortion technique that effectively renders facial images unrecognizable to the eye while maintaining their identifiability by neural network models. From the theoretical perspective, we explore how reliable state-of-the-art biometrics recognition neural networks are by checking the maximal degree of image distortion, which leaves the predicted identity unchanged. On the other hand, applying this technique demonstrates a practical solution to the engineering challenge of balancing security, precision, and performance in biometric authentication systems. Through experimenting on the widely used datasets, we assess the effectiveness of our method in preserving AI feature representation and distorting relative to conventional metrics. We also compare our method with previously used approaches. We publically release the source code for this study¹.

*Corresponding author

Email addresses: `zamdmytro@gmail.com` (Dmytro Zakharov),
`kuznetsov@karazin.ua` (Oleksandr Kuznetsov), `emanuele.frontoni@unimc.it`
(Emanuele Frontoni)

¹<https://github.com/ZamDimon/distortion-generator/tree/v1.0.0>

Table 1: An example of using our proposed image distortion technique on images from *MNIST* (Deng, 2012) and *LFW* (Huang et al., 2007) datasets. While authentic and generated images significantly differ, the feature vectors of both images in pairs are relatively close.



Keywords:

Cancelable Biometrics, Deep Learning, Triplet Loss, Feature Extraction, Convolutional Neural Networks, Information Security

1. Introduction

In the digital age, one cannot overstate the necessity for robust cybersecurity systems. With the rapid proliferation of digital identities and the increasing reliance on virtual platforms for many activities, safeguarding personal and organizational data has become a crucial problem (Hamme et al., 2022). This surge in digitalization has simultaneously amplified cybersecurity vulnerabilities, making exploring innovative and effective security solu-

tions essential. Biometric technologies, utilizing unique physical or behavioral characteristics for identification and authentication, have emerged at the forefront of this endeavor (Amin et al., 2014).

Current biometric systems, while revolutionary in many respects, have their drawbacks. A predominant concern is the risk of irreversible compromise; once a biometric trait is exposed or stolen, it is compromised forever, unlike traditional passwords or tokens that can be easily changed (Galbally et al., 2007). Furthermore, issues like data privacy, susceptibility to spoofing attacks, and the challenge of maintaining high accuracy under varied conditions underscore the limitations of existing biometric technologies. Integrating these systems into diverse platforms also presents challenges in terms of scalability, interoperability, and user accessibility.

Against this backdrop, our research introduces a new concept in biometric technologies to redefine the approach to biometric data security and management. The core of our vision is the development of novel intellectual biometric technologies that address the existing challenges and open new horizons in cybersecurity. This approach pivots on leveraging deep learning and machine learning algorithms to enhance the security and efficacy of biometric systems.

The primary objective of this research is to explore and validate the feasibility of an image distortion technique while preserving the feature vectors. This system represents a paradigm shift in biometric authentication, focusing on maintaining the original quality of biometric data while ensuring its security and privacy. Our approach diverges from traditional methods by avoiding the distortion of original biometric data, instead employing advanced AI algorithms for data analysis and template generation.

Our methodology involves an analysis of biometric data integrity and the application of state-of-the-art AI techniques. We utilize the idea of Triplet Networks to develop a sophisticated metric for biometric data comparison, ensuring the security of the data while maintaining its original characteristics. The research encompasses a series of experiments using the *MNIST* (Deng, 2012) and *LFW* (Huang et al., 2007) dataset to validate our system’s effectiveness empirically.

This research contributes significantly to the field of biometric security. By introducing a non-distortive approach to cancelable biometrics, we provide a solution that balances the need for safety with the imperative of protecting individual privacy. Our findings could influence future developments in biometric authentication, paving the way for more secure and privacy-

conscious systems.

The paper is structured to explore each aspect of the proposed system systematically. Following this introduction, we delve into the theoretical framework, experimental methodology, results analysis, and a comprehensive discussion of our research’s implications and future directions.

2. State of the Art

Our study stands out in the realm of biometric security by offering a novel AI-driven solution that not only ensures high levels of security and privacy but also addresses operational and scalability challenges inherent in current systems. This holistic approach positions our research as a significant contribution to the field, filling gaps left by previous studies and extending the applicability and efficiency of cancelable biometrics across various biometric modalities.

[Bansal and Garg \(2022\)](#) introduced a cancelable biometric template protection scheme combining format-preserving encryption with Bloom filters. This method enhances security while maintaining recognition performance. However, it primarily focuses on the encryption aspect without addressing the potential complexities involved in the operational deployment of such systems across diverse platforms. Our research aims to simplify operational challenges by utilizing AI algorithms, thereby filling this gap.

[Helmy et al. \(2022\)](#) proposed a novel hybrid encryption framework based on Rubik’s cube technique for cancelable biometric systems. Their approach showcases an innovative method to secure multi-biometric systems. However, the research is heavily centered on encryption techniques, potentially overlooking the ease of integration and scalability. Our study contributes by emphasizing a more integrated approach where security is achieved without overcomplicating the system architecture.

[Kauba et al. \(2022\)](#) explored practical cancelable biometrics for finger vein recognition, analyzing three different approaches and their impact on recognition performance and security. While their work provides valuable insights into finger vein biometrics, it does not extensively cover other biometric modalities. Our research broadens this scope by proposing a versatile AI-driven metric applicable across various biometric modalities, thereby enhancing the applicability of cancelable biometrics.

[Nayar et al. \(2021\)](#) focused on secure cancelable palm vein biometrics using a graph-based approach. Their method provides a novel perspective

on ensuring template security. However, it is specific to palm vein biometrics and may not be directly applicable to other biometric types. Our approach offers a more universal solution, applicable across different biometric systems.

[Yang et al. \(2022b\)](#) developed a linear convolution-based cancelable fingerprint authentication system, emphasizing on safeguarding fingerprint template data. Although their approach contributes significantly to fingerprint authentication, it does not address the broader spectrum of biometric modalities. Our research fills this gap by offering a comprehensive solution that is adaptable to various biometric types.

In their study, Wang, Deng, and Hu [Wang et al. \(2017b\)](#) innovatively applied a partial Hadamard transform to cancelable biometrics, enhancing the security of binary biometric representations. Their method effectively prevents the reconstruction of original data, addressing a significant security concern in binary biometric systems. Our research extends their foundational work by integrating AI algorithms, broadening the scope to various biometric modalities and focusing on preserving the original data’s integrity, thereby filling a crucial gap in user-friendly and secure biometric authentication.

In their study, [Yang et al. \(2021\)](#) addressed the vulnerability of traditional random projection-based cancelable biometrics to attack via record multiplicity (ARM). While their feature-adaptive random projection method enhances security, the focus remains narrow, primarily addressing one specific type of attack. Our research contributes by introducing a holistic approach that encapsulates broader security concerns while ensuring high recognition accuracy.

[Akdogan et al. \(2018\)](#) proposed two novel biometrics-based secure key agreement protocols, focusing on integrating cancelability in biometric data. Their approach, particularly in the SKA-CB protocol, underscores the importance of cancelable biometrics in enhancing security. However, their focus on key agreement protocols leaves a gap in broader application contexts, such as operational flexibility and cross-platform adaptability. Our research addresses these broader aspects, offering a more versatile solution in various biometric applications.

[Kaur and Khanna \(2020\)](#) emphasized the privacy and security in network/cloud-based remote biometric authentication, combining cancelable pseudo-biometric identities with secret sharing. While this approach addresses some key security concerns, it primarily focuses on remote authentication, leaving room for improvement in terms of local system integration and broader biometric modalities. Our research fills these gaps by proposing a system that is

equally effective in both local and remote contexts and across various biometric types.

[Kausar \(2021\)](#) introduced an iris-based cancelable biometric cryptosystem for securing healthcare data on smart cards, combining biometrics with symmetric key cryptography. This approach offers an interesting perspective on biometric data security in healthcare. However, the focus on iris biometrics and healthcare applications indicates a need for a more generalized approach that can be applied across different sectors. Our research responds to this need by offering a generalizable and adaptable solution in Non-Distortive Cancelable Biometrics.

[Lee et al. \(2021\)](#) proposed a tokenless cancellable biometrics scheme for multimodal biometric systems, focusing on biometric template protection without relying on tokens. Their approach is innovative in enhancing security while simplifying the authentication process. However, their research does not address the operational complexities related to the integration of such systems across various platforms. Our study aims to provide a comprehensive solution that simplifies integration and operational aspects in various application scenarios.

[Murakami et al. \(2019\)](#) developed a cancelable biometric scheme for fast and secure biometric identification, focusing on correlation-invariant random filtering. While their approach is innovative in terms of security and computational efficiency, it primarily targets large-scale identification systems. Our research complements this by offering a scalable and adaptable solution that caters to both large-scale and individualized biometric authentication needs.

[Yang et al. \(2018\)](#) focused on a cancelable multi-biometric system combining fingerprint and finger-vein biometrics. Their approach to multi-biometric systems underscores the importance of feature-level fusion for enhanced recognition accuracy and security. However, their focus is somewhat narrow, mainly on fingerprint and finger-vein biometrics. Our research expands on this by developing a framework applicable to a wider range of biometric modalities, enhancing versatility and applicability in diverse scenarios.

In summary, while these studies contribute significantly to the field of cancelable biometrics, each focuses on specific aspects or applications. Our research seeks to bridge these gaps by providing a comprehensive, scalable, and adaptable solution that enhances security, operational efficiency, and applicability across various biometric modalities and application scenarios.

3. Background

3.1. Image Distortion Techniques

Currently, as outlined in Zhang et al. (2016), image security research resolves around the following primary topics:

1. **Steganography:** Hiding information inside the cover image that is unrecognizable for a human eye (Subramanian et al., 2021; Yang et al., 2022a). Currently, as seen in (Subramanian et al., 2021), many neural network architectures are capable of resolving this problem.
2. **Cancelable Biometrics:** The uninvertible image conversion into the unrecognizable representation that can be further compared with another similarly converted image directly.
3. **Image Encrypting:** The process of converting an image to another unrecognizable representation that is decodable to a trusted party. In this case, two encoded images cannot be compared without decoding them (Zhang et al., 2016; Bok-Min et al., 2021; Matoba et al., 2009).

Our research is best related to the second and third topics. Therefore, we focus on a comparison of these two subjects. We discuss the advantages of our approach by considering an example of building the most simplistic authorization system, which all these methods are intended for in the first place.

First, consider the flow of a *user registration*, depicted in Figure 1. Suppose some user wants to use a facial recognition authorization feature on account. In that case, the system must be provided with the biometrics data, which is then processed by a generator function \mathcal{G} . *Cancelable biometrics* converts this image to another representation that will look almost the same if the same person takes another photo. *Image encrypting* will convert an image to a seemingly random format, but which can be decoded using \mathcal{G}^{-1} which is known to the trusted party (in our particular case, for the system itself). Either way, the processed data gets saved in the database, which we call a “template” data T .

Now, consider the setting where a user passes an image X , and the system wants to verify that the user exists in the database. Specifically, we need an algorithm to output 1 if X belongs to the same person as some template T from the database and 0 to different people. Here comes the main difference between the methods considered.

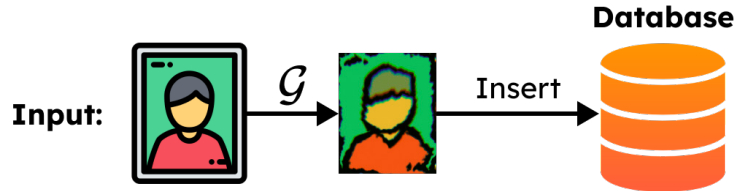


Figure 1: Facial recognition feature registration flow.

Consider cases (a) and (b) in Figure 2, where we depict the login flows for cancelable biometrics and image encoding-based approaches, respectively. In both cases, we use a metric of image comparison, or in our particular case, image distance d . As the simplest example, d might be an Euclidean or Hamming metric or can encapsulate some complex mechanism such as an image-matching technique. Now, we explain the flows for each of the cases:

- In *cancelable biometrics* approach we need to firstly generate an image $\mathcal{G}(X)$ and compare it with T using distance d . If $d(\mathcal{G}(X), T)$ is small enough, we consider ownership of both X and T to be the same.
- In *image encoding* approach, we retrieve the original image from the template $\mathcal{G}^{-1}(T)$ and compare it to X . If $d(\mathcal{G}^{-1}(T), X)$ is small enough, we again consider the ownership of X and T to be the same.

Note that in both cases, we need to conduct two steps: first, either apply \mathcal{G} or \mathcal{G}^{-1} , and then compare two images using d . We propose a novel approach depicted as the case (c) in Figure 2. In our implementation, we can directly compare X and T using the secret comparison metrics d^* unknown to the external user. This way, we can directly find $d^*(X, T)$ without any image transformations, which is costly for any system. Simultaneously, the traditional metric d between X and T would remain very large, making it impossible or very complicated to determine how close X and T are.

3.2. Triplet Loss Usage for training an Embedding Model

Denote by \mathcal{I} a set of images. To further avoid confusion with terminology, we define the term *embedding model* as the function $\mathcal{F} : \mathcal{I} \rightarrow \mathbb{R}^m$, which maps an image to a low-dimensional representation in \mathbb{R}^m , sometimes called a *feature vector*.

The embedding model is an excellent tool for various problems, not only in terms of computational efficiency but also since we can encapsulate core

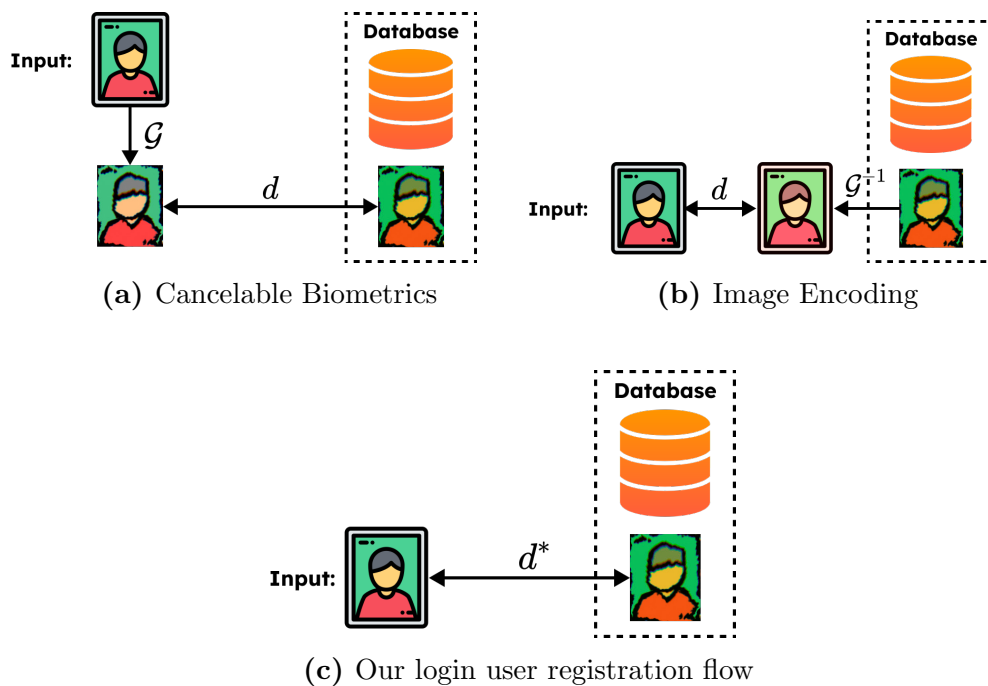


Figure 2: Comparison of different login flows using biometrics data, where \mathcal{G} denotes the generation function, d denotes the traditional image distance metrics, while d^* – a secret one. In flow (a), we first generate a distorted image and compare it with a template. In flow (b), we find the inverse of a template and compare it with an input. In our proposed flow (c), we compare template and image directly.

patterns in data using only hundreds of numbers (instead of ten thousands of them). For example, consider papers (Spruyt, 2018) and (Guo et al., 2022), where embeddings store information about geographical position (for more examples, see subsection 3.3).

Denote by $\theta_{\mathcal{F}}$ parametrization of an embedding model \mathcal{F} . Similarly to *FaceNet* paper by Schroff et al. (2015), we limit the output to the unit hypersphere $S^{m-1} \triangleq \{\mathbf{x} \in \mathbb{R}^m : \|\mathbf{x}\|_2 = 1\}$ with the embedding size of m . This step is optional, though: in fact, any function \mathcal{F} might be provided, not limited to deep learning ones, as long as the gradient descent algorithm can be applied.

The main purpose of our neural network is to create “similar” embeddings for images from the same class and “different” for ones from different classes. We define the measure of “distinctiveness” as follows:

$$d_{\mathcal{F}}(X, Y) \triangleq \|\mathcal{F}(X) - \mathcal{F}(Y)\|_2^2. \quad (1)$$

This way, if X_1 and X_2 belong to the same class, while Y to a different one, $d_{\mathcal{F}}(X_1, X_2)$ must be much smaller than both $d_{\mathcal{F}}(X_1, Y)$ and $d_{\mathcal{F}}(X_2, Y)$.

However, the neural network must know how to learn to produce such embeddings. For that reason, we consider the dataset $\mathbb{T} = \{(A_i, P_i, N_i)\}_{i=0}^{n_T}$ where A_i and P_i are images from the same class (called *anchor* and *positive* images, respectively) whereas N_i from a different one (called *negative* image).

The idea of triplet loss is to constraint an embedding of an anchor image A to be closer to the corresponding embedding of P than to an image N by a positive value μ (called *margin*). So ideally, for all triplets $(A, P, N) \in \mathbb{T}$ we want:

$$d_{\mathcal{F}}(A, P) < d_{\mathcal{F}}(A, N) - \mu \quad (2)$$

From the probabilistic perspective, suppose that we take samples $\mathbf{T} = (A, P, N)$ from a true distribution p_{data} . Our goal is to maximize the probability of the aforementioned relationship:

$$\max_{\mathcal{F}} \mathbb{P}_{(A,P,N) \sim p_{\text{data}}} [d_{\mathcal{F}}(A, P) < d_{\mathcal{F}}(A, N) - \mu] \quad (3)$$

Practically, the following loss function is considered, which is called a *triplet loss function*:

$$\ell_{\text{triplet}}(\mathbf{T}; \mathcal{F}) \triangleq \text{ReLU}(d_{\mathcal{F}}(A, P) - d_{\mathcal{F}}(A, N) + \mu), \quad (4)$$

and then $\mathbb{E}_{\mathbf{T} \sim p_{\text{data}}} [\ell_{\text{triplet}}(\mathbf{T}; \mathcal{F})]$ is minimized w.r.t. \mathcal{F} .

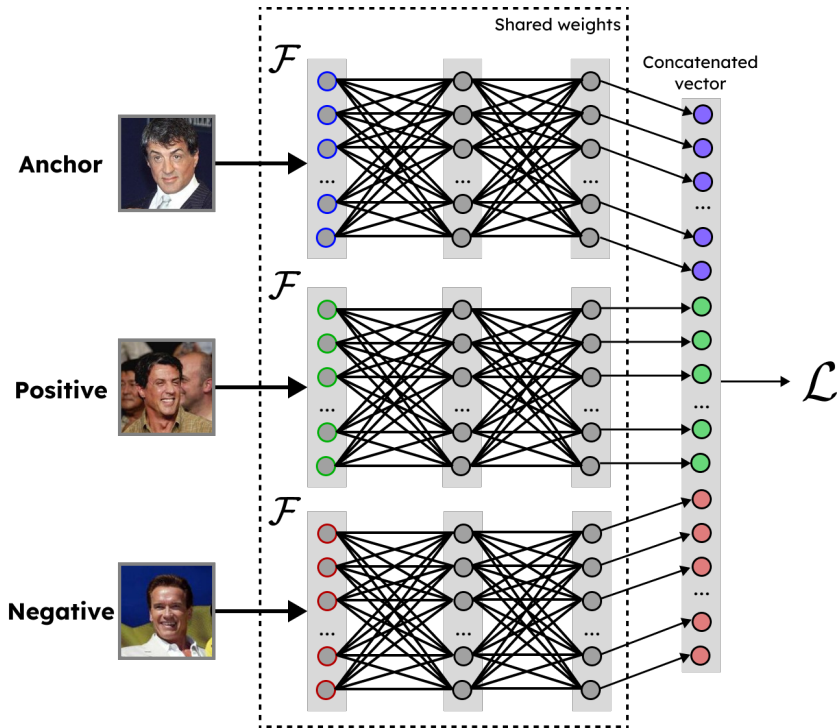


Figure 3: Triplet Network architecture. We input three images (anchor, positive, and negatives), then using embedding model \mathcal{F} with shared parameters retrieve three feature vectors, and then concatenate them to get the loss value.

3.3. Triplet Network

Triplet loss and triplet neural networks play a crucial role in many areas of computer vision: for instance, they are used in face recognition (Schroff et al., 2015; Wang et al., 2017a), person reidentification (Zhang et al., 2018), object tracking (Dong and Shen, 2018), and even generative neural networks (Cao et al., 2017).

To examine the structure of a triplet neural network, we refer to Figure 3.

Triplet Network uses three copies of an embedding model with shared parameters (Hoffer and Ailon, 2015). Using the triplet loss defined in subsection 3.2, we calculate the loss and update the weights of an embedding model. We can then safely retrieve and use the embedding model for our purposes. Specifically, the most basic example algorithm is outlined in Algorithm 1.

Algorithm 1 The simplest training algorithm of embedding model using triplet network architecture.

- for** each batch $\mathbb{B} = \{(A_i, P_i, N_i)\}_{i=1}^{n_B} \subset \mathcal{T}$ **do**
1. Find embeddings $\{\mathcal{F}(A_i), \mathcal{F}(P_i), \mathcal{F}(N_i)\}_{i=1}^{n_B}$.
 2. Concatenate them: $V \leftarrow \{\mathcal{F}(A_i) \oplus \mathcal{F}(P_i) \oplus \mathcal{F}(N_i)\}_{i=1}^{n_B}$.
 3. Find the batch loss $\mathcal{L}(\theta_F; \mathbb{B}) \leftarrow \frac{1}{n_B} \sum_{\mathbf{v} \in V} \ell(\mathbf{v})$ where

$$\ell(\mathbf{v}) = \|\mathbf{v}_{0:m} - \mathbf{v}_{m:2m}\|_2^2 - \|\mathbf{v}_{0:m} - \mathbf{v}_{2m:3m}\|_2^2 + \mu.$$

4. Update θ_F using the gradient descent. For example, in its simplest form we use

$$\theta_F^{(j+1)} \leftarrow \theta_F^{(j)} - \eta \nabla_{\theta_F} \mathcal{L}(\theta_F^{(j)}; \mathbb{B}).$$

end for

4. Methods

4.1. Overview

Distortion generator is a function $\mathcal{G} : \mathcal{I} \rightarrow \mathcal{I}$, which generates a distorted image from a given one. This generator must meet the following two criteria:

1. Difference between images $\mathcal{G}(X)$ and X is as large as possible. We call the metrics for such difference $d_{\text{img}} : \mathcal{I} \times \mathcal{I} \rightarrow \mathbb{R}_{\geq 0}$.
2. Difference between embeddings $\mathcal{F} \circ \mathcal{G}(X)$ and $\mathcal{F}(X)$ is as small as possible. We call the metrics for this difference $d_{\text{emb}} : \mathbb{R}^m \times \mathbb{R}^m \rightarrow \mathbb{R}_{\geq 0}$.

Suppose inputs are taken from the true distribution p_{data} . This way, informally, we want to have:

$$\max_{\mathcal{G}} \mathbb{E}_{X \sim p_{\text{data}}} [d_{\text{img}}(\mathcal{G}(X), X)] \tag{5}$$

$$\text{while } \min_{\mathcal{G}} \mathbb{E}_{X \sim p_{\text{data}}} [d_{\text{emb}}(\mathcal{F} \circ \mathcal{G}(X), \mathcal{F}(X))] \tag{6}$$

Note that in this case, we cannot employ the idea of a two-player minimax game used in GAN (Goodfellow et al., 2014) directly since we cannot modify the embedding neural network \mathcal{F} , although this idea does seem attractive at first glance.

However, if we wanted to train a pair $(\mathcal{F}, \mathcal{G})$ together, that could be possible. That being said, that is a great topic for future research, but for now we restrict ourselves \mathcal{F} to be fixed.

4.2. Loss Function

To represent the optimization problem above, we define the following loss function for a single image:

$$\ell(X; \mathcal{G}, \mathcal{F}) \triangleq (1 - \pi_{\text{emb}}) \cdot \ell_{\text{img}}(X; \mathcal{G}) + \pi_{\text{emb}} \cdot \ell_{\text{emb}}(X; \mathcal{G}, \mathcal{F}), \quad (7)$$

where $\pi_{\text{emb}} \in [0, 1]$ is a positive hyperparameter, regulating the importance of ℓ_{emb} in contrast to ℓ_{img} .

We define the two loss components as follows:

$$\ell_{\text{img}}(X; \mathcal{G}) \triangleq -d_{\text{img}}(\mathcal{G}(X), X), \quad (8)$$

$$\ell_{\text{emb}}(X; \mathcal{G}, \mathcal{F}) \triangleq \text{ReLU}(d_{\text{emb}}(\mathcal{F} \circ \mathcal{G}(X), \mathcal{F}(X)) - \alpha). \quad (9)$$

Note that ℓ_{img} is always negative since we want to *maximize* the difference between images. Also, we decide to use $\text{ReLU}(d_{\text{emb}}(\cdot) - \alpha)$ for ℓ_{emb} instead of $d_{\text{emb}}(\cdot)$ since otherwise neural network might focus primarily on reducing the distance between embeddings. However, if we use the ReLU function, we do not punish the neural network for an embedding difference unless it exceeds α . In this sense, α also serves as a parameter that regulates how well we want our generator to fit embeddings: the larger α is, the more distinct images are according to metrics d_{img} , but less similar according to d_{emb} (see [subsection 6.3](#)).

Let us now choose the concrete expressions for distances. We use $d_{\mathcal{F}}$ from [Equation 1](#) for the embedding difference:

$$d_{\text{emb}}(X; \mathcal{G}, \mathcal{F}) \triangleq d_{\mathcal{F}}(\mathcal{G}(X), X) = \|\mathcal{F} \circ \mathcal{G}(X) - \mathcal{F}(X)\|_2^2. \quad (10)$$

Choosing d_{img} is trickier. In the following subsections, we discuss several choices.

4.2.1. L1 Distance

One of the most widely used ([Le and Samaras, 2019](#); [Liu et al., 2021](#); [Isola et al., 2016](#)) loss function for image generations tasks is the L_1 distance between the ground truth and generated images:

$$\|X, Y\|_1 \triangleq \sum_{i=1}^W \sum_{j=1}^H \sum_{k=1}^{n_C} |X_{ijk} - Y_{ijk}| \quad (11)$$

We will define the distance between images as the average distance, similarly to MSE:

$$d_{\text{img}}^{(L_1)}(\hat{X}, X) = \frac{\|\hat{X}, X\|_1}{W \cdot H \cdot n_C}, \quad (12)$$

where $W \times H \times n_C$ is the image shape, and by \hat{X} we denote the predicted value. In contrast to L_2 distance, which we define in the next subsection, L_1 encourages less blurring.

4.2.2. L_2 Distance

L_2 distance is also frequently used in image generations tasks (Vasluianu et al., 2021; Gatys et al., 2016). For grayscale images, it is defined as $\|X - Y\|_F$, where $\|\cdot\|_F$ denotes the Frobenius norm. For RGB images, similarly to Equation 11, we define the L_2 distance as follows:

$$\|X, Y\|_2 = \left(\sum_{i=1}^W \sum_{j=1}^H \sum_{k=1}^{n_C} (X_{ijk} - Y_{ijk})^2 \right)^{1/2} \quad (13)$$

The distance between images is in turn defined as the MSE value:

$$d_{\text{img}}^{(L_2)}(\hat{X}, X) = \frac{\|\hat{X}, X\|_2^2}{W \cdot H \cdot n_C} \quad (14)$$

4.2.3. DSSIM

However, there are multiple ways for a neural network to “cheat” in this case. For instance, the neural network might invert background pixels or reduce pixels’ intensities since that would not affect embeddings drastically, which in turn will not increase d_{emb} . For this reason, we decided to try using the more advanced method such as a SSIM(X, Y) (structural similarity index measure) metrics as suggested by (Zhao et al., 2017). It is defined as:

$$\text{SSIM}(X, Y) = \frac{(2\mu_X\mu_Y + \kappa_1)(2\sigma_{XY} + \kappa_2)}{(\mu_X^2 + \mu_Y^2 + \kappa_1)(\sigma_X^2 + \sigma_Y^2 + \kappa_2)}, \quad (15)$$

where μ_X, μ_Y are pixel sample means, σ_X^2, σ_Y^2 are variances, $\sigma_{XY} = \text{cov}[X, Y]$ is a covariance, and κ_1, κ_2 are constants to stabilize the division.

The distance measure, called ‘‘structural dissimilarity’’ (DSSIM)², in turn, is defined as

$$d_{\text{img}}^{(\text{DSSIM})}(\hat{X}, X) \triangleq \frac{1 - \text{SSIM}(\hat{X}, X)}{2}, \quad (16)$$

with a range $[0, 1]$.

4.2.4. Sobel Distance

After experiments, we decided to employ another loss function, which, combined with L_1 loss, performed best on the LFW dataset. Suppose we get an image I as an input. We use two kernels:

$$\mathcal{K}_x = \begin{bmatrix} -1 & 0 & 1 \\ -2 & 0 & 2 \\ -1 & 0 & 1 \end{bmatrix}, \quad \mathcal{K}_y = \begin{bmatrix} 1 & 2 & 1 \\ 0 & 0 & 0 \\ -1 & -2 & -1 \end{bmatrix}. \quad (17)$$

Then, using these two kernels, we find the mask (all operations are performed elementwise):

$$\mathcal{S}(I) = \sqrt{(\mathcal{K}_x * I)^2 + (\mathcal{K}_y * I)^2}. \quad (18)$$

Essentially, $\mathcal{S}(I)$ gives a map of regions of I which contain edges. Finally, we define the distance measure as follows:

$$d_{\text{img}}^{(\text{sobel})}(\hat{X}, X) = \left\| \mathcal{S}(X) \odot \hat{X}, \mathcal{S}(X) \odot X \right\|_1. \quad (19)$$

The difference between this loss and one specified in [subsubsection 4.2.1](#) is that we account for the loss only in those regions where there are edges since using the pure L_1 distance does not restrict the neural network from simply changing the content inside the face without bothering about the shape.

4.2.5. Combined Distance

Combined loss is just a linear combination of several distances. The best results were achieved by combining the L_1 distance (see [subsubsection 4.2.1](#)) and Sobel distance (see [subsubsection 4.2.4](#)):

$$d_{\text{img}}^{(\text{comb})}(\hat{X}, X) = \omega \cdot d_{\text{img}}^{(L_1)}(\hat{X}, X) + (1 - \omega) d_{\text{img}}^{(\text{sobel})}(\hat{X}, X), \quad (20)$$

where by regulating ω we can adjust the importance of $d_{\text{img}}^{(L_1)}$ relative to $d_{\text{img}}^{(\text{sobel})}$. In our experiments, we use $\omega = 0.5$.

²Note that rigorously speaking, this is not a distance function since triangle inequality is not necessarily satisfied. However, this is not a problem for us if we use this expression as a loss function.

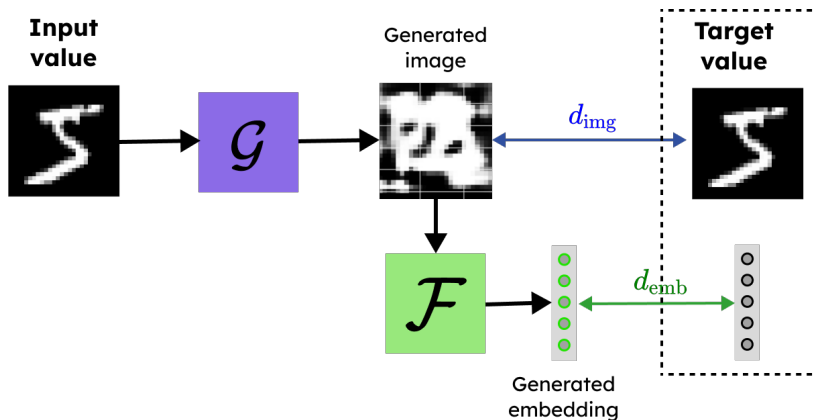


Figure 4: Trainer Network architecture.

4.3. Trainer Network Architecture

When we finally defined the loss $\ell(X; \mathcal{G}, \mathcal{F})$, we need to train our generator to minimize this expected loss, that is:

$$\hat{\mathcal{G}} = \arg \min_{\mathcal{G}} \mathbb{E}_{X \sim p_{\text{data}}} \ell(X; \mathcal{G}, \mathcal{F}) \quad (21)$$

To achieve this, inspired by [Zhmoginov and Sandler \(2016\)](#), we create a helper network, which we call a *Trainer Network*. Its architecture is depicted in the [Figure 4](#).

For training, we form the dataset in a form $\{(X_i, (X_i, \mathcal{F}(X_i)))\}_{i=1}^N$ where the input is an image X_i and output is a pair of this same image together with its embedding $\mathcal{F}(X_i)$.

The trainer network takes an image X , generates an image $\mathcal{G}(X)$, and then takes the embedding of this image $\mathcal{F} \circ \mathcal{G}(X)$. It then outputs both values and applies the loss from [Equation 7](#) (since the target value has the same shape). Note that we freeze the embedding network \mathcal{F} and make only \mathcal{G} 's weights trainable.

5. Implementation

In this section, we specify the architecture used for training our models on *MNIST* and *LFW* datasets.

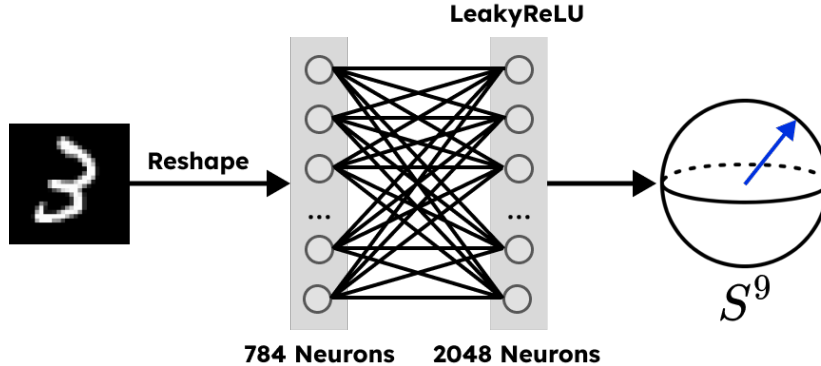


Figure 5: Embedding model architecture. S^9 denotes the layer with 10 neurons which then gets L_2 normalized.

5.1. Embedding Model

For the *LFW* dataset, we use the pre-trained *FaceNet* architecture. We decided to employ this architecture since it provides one of the best values of accuracy in the face recognition task: namely, 98.87% for fixed center cropping, and 99.63% for the extra face alignment (see original paper (Schroff et al., 2015) for reference). Note that any other embedding neural network might be used, such as *VGGFace* (Parkhi et al., 2015), for example.

For the *MNIST* dataset, we build our own embedding model. For that, we use the architecture specified in Figure 5.

We use the LeakyReLU function defined as $x \mapsto \max\{\alpha x, x\}$ (for $\alpha < 1$). We choose $\alpha = 0.01$. For the output layer, we do not use an activation function; instead, we normalize the retrieved vector by using $\mathbf{x} \mapsto \frac{\mathbf{x}}{\sqrt{\|\mathbf{x}\|_2^2 + \epsilon}}$ for sufficiently small $0 < \epsilon \ll 1$. As a weight initializer, we use the *He initialization* (Kumar, 2017), which initializes weights according to the normal distribution $\mathcal{N}\left(0, \frac{1}{n_L}\right)$ where n_L is the number of nodes feeding into the layer. We choose our embedding dimensionality to be $m = 10$. We then apply the training algorithm described in subsection 3.3 using margin $\mu = 0.2$ and a learning rate of $\eta = 5 \cdot 10^{-5}$ using *Adam* optimizer (Kingma and Ba, 2014).

5.2. Generator Model

For the generator model, we decided to employ the *U-Net* architecture (Ronneberger et al., 2015), and get the structure specified in Figure 6 for the

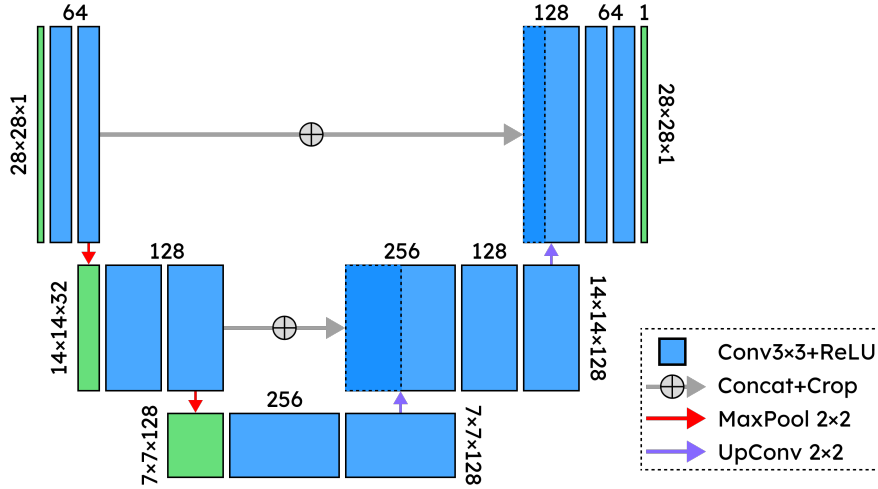


Figure 6: Generator model architecture for the *MNIST* dataset based on *U-Net*.

MNIST dataset (architecture for the *LFW* dataset is the same with the only difference in shapes). Similarly to the embedding model from [subsection 5.1](#), we use *He* weights initialization, LeakyReLU activation for all convolutional layers except for the last one, and the *sigmoid function* before the output to map pixel values to the interval $(0, 1)$. We use batch size of 64 with a learning rate $\eta = 10^{-4}$. Other parameters depend on the dataset:

- For the *MNIST* dataset, we use a margin $\alpha = 0.3$, $\pi_{\text{emb}} = 0.9$, and L_2 distance as the loss function (see [subsection 4.2.2](#)).
- For the *LFW* dataset, we use a margin $\alpha = 0.2$, $\pi_{\text{emb}} = 0.1$, and the combined distance (see [subsection 4.2.5](#)).

6. Results

In this section, we analyze the efficacy of the proposed approach after training the neural networks.

6.1. Image Distance Comparison

Despite the noticeable changes between the original and generated images, depicted in the [Table 1](#), we still need to provide a quantitative representation of the difference. We will compare images in the following three setups:

“real vs generated same class”, “real vs real different classes”, “generated vs generated different classes”. We use the L_2 distance $d_{\text{img}}^{(L_2)}$ defined in [subsubsection 4.2.2](#) as a difference metric. We get results specified in [Table 2](#).

As can be seen, the distance between authentic and generated images have significant values. Consider the *MNIST dataset* as an example: even for pairs of digit 4 with the minimum value of 0.773 and especially for digit 1 with a maximum distance of 0.886. That highlights that the neural network produced drastically different images in terms of MSE. At the same time, for the *MNIST dataset*, the mean-squared difference remained the same for “generated vs generated” pairs, indicating that generation still keeps digits close to each other. In turn, for the *LFW dataset*, the opposite holds: distances between generated faces are significant.

6.2. Image Encodings Comparison

To give an intuitive representation of predictions, we apply the PCA ([Maćkiewicz and Ratajczak, 1993](#)) and convert \mathbb{R}^m vectors to vectors \mathbb{R}^3 , which is easy to illustrate on the 3D plot.

That being said, we firstly take a batch of images $\mathbb{B} := \{X_i\}_{i=1}^{n_B}$, generate distorted images $\mathbb{B}_G = \mathcal{G}(\mathbb{B})$, and then generate two sets of embeddings: $\mathcal{F}(\mathbb{B})$ and $\mathcal{F}(\mathbb{B}_G)$. Finally, we apply the PCA to generate three-dimensional representations of \mathbb{R}^m embeddings. Results are depicted in the [Figure 7](#). As can be seen, embeddings of the same class almost do not change under the generator transformation and remain close to each other.

6.3. Dependency on the Margin Parameter

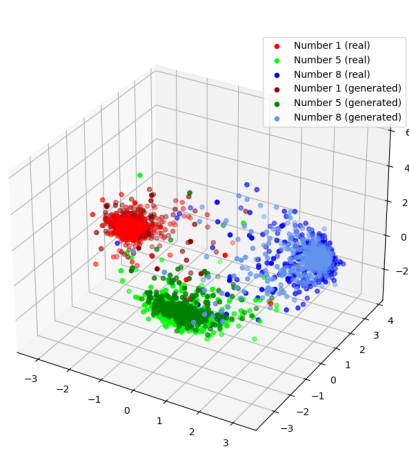
We also tried different values of α to find the best fit. Results for different values of α for the *MNIST dataset* are depicted in the [Figure 8](#).

As seen, for greater α 's, embeddings after generation become more distant from the original ones, but the image distortion is much more considerable. For instance, for $\alpha = 0.8$, embeddings of digit 1 become entirely different from the original ones, and thus this value should not be used for training. $\alpha = 0.4$ shows a slight shift of embeddings location after generation, but they still remain relatively close. In turn, $\alpha = 0$ and $\alpha = 0.1$ keep embeddings almost unchanged. In our experiments, $\alpha = 0.2$ gave us the best results, providing a sufficient trade-off between embedding and image distances.

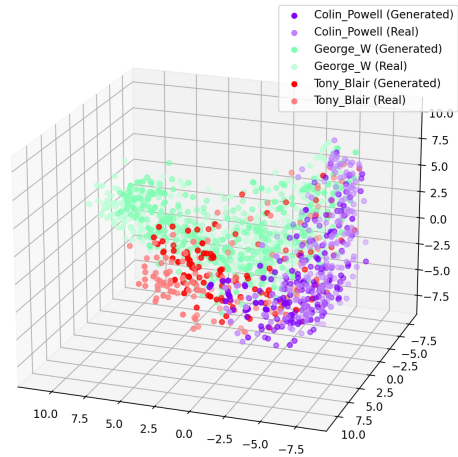
Table 2: L_2 distances between images of the same digit in three different setups specified as columns. We mark in **bold** extreme values and highlight in **green** the best result and in **orange** the worst in terms of Real-Gen distances. As can be seen for both *MNIST* and *LFW* datasets, the difference between real and generated images greatly exceeds “Real-Real” distances. We use 20% images from both datasets: approximately 2.6k images for *LFW* and 12k for *MNIST*.

Class	Real-Gen	Real-Real	Gen-Gen
0	0.791	0.129	0.082
1	0.886	0.057	0.031
2	0.850	0.128	0.108
3	0.850	0.113	0.109
4	0.773	0.104	0.049
5	0.843	0.120	0.106
6	0.826	0.112	0.058
7	0.845	0.096	0.062
8	0.838	0.115	0.087
9	0.800	0.097	0.048

Class	Real-Gen	Real-Real	Gen-Gen
George W. Bush	0.295	0.046	0.129
Colin Powell	0.267	0.042	0.132
Tony Blair	0.298	0.046	0.122
Donald Rumsfeld	0.278	0.045	0.120
Gerhard Schröder	0.293	0.043	0.107
Ariel Sharon	0.273	0.046	0.145
Hugo Chavez	0.263	0.041	0.126
Junichiro Koizumi	0.319	0.045	0.126
John Ashcroft	0.282	0.039	0.116
Jacques Chirac	0.297	0.051	0.106



(a) *MNIST* dataset



(b) *LFW* dataset

Figure 7: Embeddings of real and generated images after applying PCA for 3 batches of different classes. We used roughly 300 embeddings per class for the *MNIST* dataset and roughly 30 per person for the *LFW* dataset.

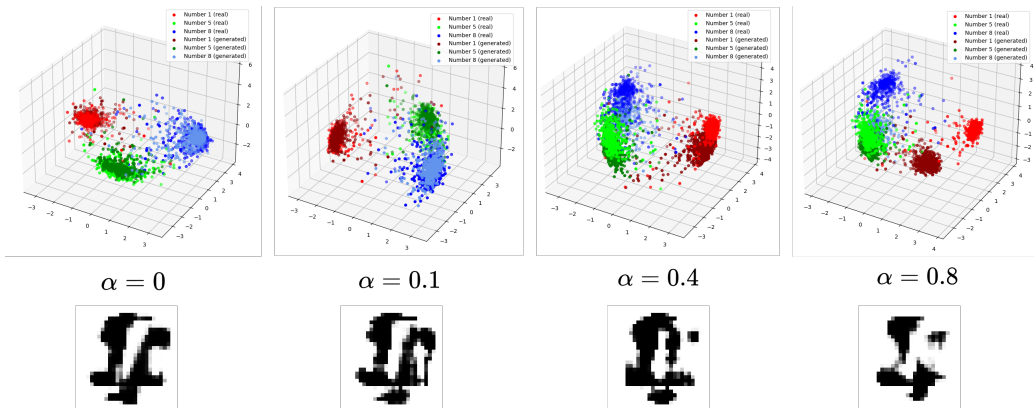


Figure 8: PCA representation of embeddings, corresponding example of a distorted digit of *1* and margin α .

6.4. Mock Recognition System

In this section, we verify that confusion matrices and ROC curves do not differ significantly if we store distorted images instead of real ones.

For that, we conduct the following experiment: we place distorted images of three classes (for *MNIST* dataset, take **1,2,3** for concreteness) in an improvised storage, being simply an in-memory hashmap in our case. Then, we:

1. take 1000 non-distorted images belonging to these three classes and try entering into the “system”;
2. take 1000 non-distorted images of any other three classes (except for previously chosen triplet) and try logging in.

We expect the former to be successful login attempts while the latter to be invalid authorizations. We then build confusion matrices by providing a number of TPs (true positives), TNs (true negatives), FPs (false positives), and FNs (false negatives). We then calculate the following metrics:

$$\text{Precision} = \frac{\text{TP}}{\text{TP} + \text{FP}}, \quad \text{Recall} = \frac{\text{TP}}{\text{TP} + \text{FN}}, \quad (22)$$

$$F_1 = \frac{2 \times \text{Precision} \times \text{Recall}}{\text{Precision} + \text{Recall}}. \quad (23)$$

We take 1000 different values for a threshold τ in range $[0, 4]$ and classify images X, Y to be of the same class if $d_{\mathcal{F}}(X, Y) < \tau$ and of different ones otherwise. We then chose a threshold that provided us with the best F_1 score and built the corresponding confusion matrix. We get results depicted in the [Table 3](#) and ROC curves depicted in [Figure 9](#).

As we can see, accuracy metrics do not differ significantly under the image distortion and therefore we have successfully achieved our goal. Moreover, the distortion-generated technique even slightly outscored the non-distortive approach.

6.5. Limitations

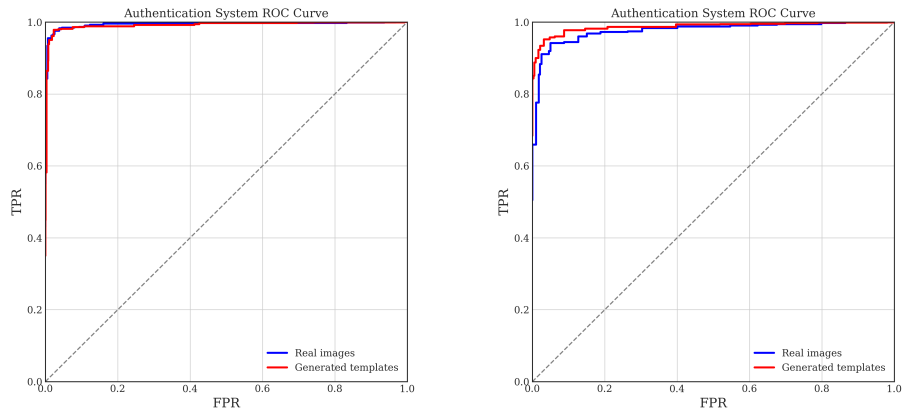
Certainly, during the training process, we encountered numerous issues and obstacles, some of which are depicted in the [Table 4](#) together with the causes. Some of them include:

- **Vanishing or exploding gradients:** the generator model produces the same blank image regardless of the input.

Table 3: Confusion matrices and metric values for authentication system with(a) and without(b) distorting original inputs.

MNIST Dataset					
(a) Without distortion			(b) With distortion		
		Prediction			
Actual		Positive	Negative	Actual	
	Positive	1174	26		Positive
Negative	29	1171	Negative	32	1168
Precision		97.59%		Precision	
Recall		97.83%		97.34% (↓ 0.25%)	
F_1 score		97.71%		97.58% (↓ 0.25%)	
				F_1 score	
				97.46% (↓ 0.25%)	

LFW Dataset					
Prediction			Prediction		
Actual		Positive	Negative	Actual	
	Positive	1130	70		Positive
Negative	80	1120	Negative	57	1143
Precision		93.34%		Precision	
Recall		94.17%		95.25% (↑ 1.91%)	
F_1 score		93.78%		95.17% (↑ 1.00%)	
				F_1 score	
				95.21% (↑ 1.43%)	



(a) *MNIST* dataset

(b) *LFW* dataset

Figure 9: ROC curve for a mock authentication system using (a) *MNIST* and (b) *LFW* datasets. Red color represents the curve for a case where we store distorted images in the storage while blue color corresponds to storing real images.




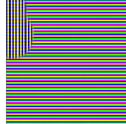


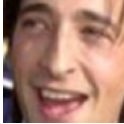





- **Highlighting the contours without concealing effect:** the generator model “cheats” by not changing the contours but instead changing the content inside them. This results in an image, from which it is easy to recognize the face.
- **Changing the color gamma:** the neural network simply changes the image’s gamma, which surely does not conceal the face.

7. Comparison to other research

In this section, we delve deeper into the comparative analysis of our Non-Distortive Cancelable Biometrics system with existing notable works in the field of biometric security. The focus is on understanding how our approach aligns with or diverges from these established methods, particularly in terms of performance metrics like the Equal Error Rate (EER).

In the comparative analysis presented in Table 5, we juxtapose the EER of various biometric authentication systems, including our own, against a backdrop of diverse datasets and biometric modalities. This table serves as

Table 4: Three primary challenges when training the generator model: vanishing gradients, highlighting the contours, and changing the color gamma, and corresponding examples with possible causes.

Problem	MNIST		LFW		Possible Cause
	Real	Generated	Real	Generated	
Vanishing or exploding gradients					<ol style="list-style-type: none"> 1. Too large learning rate. 2. Too small π_{emb} or too large α: ignoring preserving embeddings.
Highlighting the contours without concealing effect					<ol style="list-style-type: none"> 1. Too large π_{emb}: focusing too much on saving embeddings. 2. Too small α. 3. Typically happens for SSIM loss.
Changing the color gamma					<ol style="list-style-type: none"> 1. Bad balance between π_{emb}, learning rate, and α. 2. Typically happens for L_1 or L_2 loss.

a crucial benchmark, allowing us to contextualize our Non-Distortive Cancelable Biometrics system within the broader landscape of biometric security research.

Table 5: Comparative Analysis of Biometric Authentication Systems

Source	Type of Images, Dataset	EER, (%)
Yang et al. (2022b)	Fingerprint, <i>FVC2002</i>	0.5 – 4.5
Yang et al. (2022b)	Fingerprint, <i>FVC2004</i>	2.7 – 6.3
Yang et al. (2022b)	Face, <i>LFW</i>	1.9
Yang et al. (2022b)	Fingerprint, <i>FVC2002</i>	7.6 – 9.4
Yang et al. (2022b)	Fingerprint, <i>FVC2004</i>	15.6
Kaur and Khanna (2020)	Face, <i>CASIA</i>	2.2 – 9.3
Yang et al. (2021)	Fingerprint, <i>FVC2002</i>	1.0 – 4.0
Yang et al. (2021)	Fingerprint, <i>FVC2004</i>	11
Wang et al. (2017b)	Fingerprint, <i>FVC2002</i>	1.0 – 5.2
Wang et al. (2017b)	Fingerprint, <i>FVC2004</i>	13.3
Our Work	Numbers, <i>MNIST</i>	2.5
Our Work	Face, <i>LFW</i>	4.8

The work of Lee et al. (2021) in multimodal biometric systems stands out for its impressive EER range, particularly in fingerprint recognition on the *FVC2002* and *FVC2004* datasets, and facial recognition on the *LFW* dataset. Their EERs, spanning from as low as 0.5% to 6.3%, underscore the efficacy of leveraging multiple biometric modalities. This multimodal approach, by integrating diverse biometric data, enhances the overall system robustness, a feature that our system aims to emulate in a single-modality context.

Yang et al. (2022b) present a higher EER for fingerprint recognition, particularly on the *FVC2004* dataset, where the EER peaks at 15.6%. This elevated rate could be indicative of the challenges inherent in the dataset or perhaps limitations in the methodological approach they employed. In contrast, our system, while not directly comparable due to different modalities, shows a more favorable EER of 4.8% for facial recognition on the *LFW* dataset, suggesting a more robust performance in handling biometric variability.

Kaur and Khanna (2020) explore facial biometrics using the *CASIA* dataset, with their EER ranging from 2.2% to 9.3%. The broad range of

their EER might reflect the varying complexities within the dataset and the adaptability of their system to different facial features. Our system, while tested on a different facial dataset (*LFW*), demonstrates a competitive edge with a consistent EER, highlighting its potential for reliable performance across diverse facial data.

The studies by [Yang et al. \(2021\)](#) and [Wang et al. \(2017b\)](#) focus on fingerprint biometrics, with EERs that offer a balanced perspective on security and usability. [Yang et al. \(2021\)](#) report EERs ranging from 1.0% to 4.0% for *FVC2002* and 11% for *FVC2004*, while [Wang et al. \(2017b\)](#) present EERs from 1.0% to 5.2% for *FVC2002* and 13.3% for *FVC2004*. These results, though specific to fingerprint biometrics, provide valuable insights into the efficacy of different biometric processing techniques, which are instrumental in guiding our approach to facial biometric authentication.

Our work, with an EER of 2.5% on the *MNIST* dataset and 4.8% on the *LFW* dataset, demonstrates a promising balance between security and usability. The *MNIST* dataset, though less complex, serves as a foundational testbed, validating the core principles of our approach. The *LFW* dataset, more representative of real-world scenarios, further affirms the robustness and applicability of our system in a practical context.

In summary, our comparative analysis not only situates our Non-Distortive Cancelable Biometrics system within the current state of biometric security research but also highlights its potential as a competitive and innovative solution. By maintaining the integrity of original biometric data and leveraging advanced AI algorithms, our system emerges as a promising candidate for future biometric authentication applications, balancing the dual imperatives of security and user convenience.

8. Conclusion

This paper has presented a novel approach to biometric security that maintains the integrity of original biometric data while ensuring robust security and privacy. The experimental results, leveraging the *MNIST* and *LFW* datasets and advanced deep learning algorithms, have demonstrated the feasibility and effectiveness of this innovative system.

Key findings include:

- **Feasibility of Non-Distortive Approach.** The experiments have successfully shown that it is possible to generate cancelable biometric

templates that retain high similarity in AI metrics while appearing significantly different in traditional metrics. This finding is crucial as it validates the core premise of the Non-Distortive Cancelable Biometrics system.

- **AI-Driven Metric Similarity.** AI algorithms, particularly convolutional neural networks, have proven effective in maintaining metric similarity between the original and transformed biometric data. This aspect underscores the potential of AI in enhancing biometric security.
- **Security and Privacy.** The system's ability to generate non-invertible and non-replicable biometric templates addresses significant concerns regarding data security and user privacy in traditional biometric systems.
- **Operational Flexibility.** The adaptability of the system to various biometric modalities and its scalability across different platforms.

The promising results of this study pave the way for further research and development in this field. Future work could focus on:

- **Enhancing AI Algorithms.** Continuous improvement of the AI algorithms for more nuanced feature extraction and comparison.
- **Expanding Biometric Modalities.** Exploring the application of this system to other biometric data types such as voice recognition or gait analysis.
- **Real-World Implementation.** Testing the system in real-world scenarios to assess its practicality and performance under varied conditions.

In conclusion, the Non-Distortive Cancelable Biometrics system represents a significant step forward in biometric security. Its ability to balance security, privacy, and operational efficiency sets a new benchmark for future biometric systems. The insights from this research contribute substantially to the ongoing discourse in biometric technology, offering a viable and innovative solution to the challenges faced in this rapidly evolving field.

9. CRediT authorship contribution statement

Dmytro Zakharov: Methodology, Writing–original draft. Oleksandr Kuznetsov: Conceptualization & Data curation, Writing – review & editing. Emanuele Frontoni: Investigation & Supervision.

10. Declaration of competing interest

The authors declare that they have no known competing financial interests or personal relationships that could have appeared to influence the work reported in this paper.

11. Data availability

Data will be made available on request.

12. Acknowledgement

- This project has received funding from the European Union’s Horizon 2020 research and innovation programme under the Marie Skłodowska-Curie grant agreement No. 101007820 - TRUST. This publication reflects only the author’s view and the REA is not responsible for any use that may be made of the information it contains.
- This research was funded by the European Union – NextGenerationEU under the Italian Ministry of University and Research (MIUR), National Innovation Ecosystem grant ECS00000041-VITALITY-CUP D83C22000710005.

References

- Akdogan, D., Karaoglan Altop, D., Eskandarian, L., Levi, A., 2018. Secure key agreement protocols: Pure biometrics and cancelable biometrics. *Computer Networks* 142, 33–48. doi:[10.1016/j.comnet.2018.06.001](https://doi.org/10.1016/j.comnet.2018.06.001).
- Amin, R., Gaber, T., ElTaweel, G., Hassanien, A.E., 2014. Biometric and traditional mobile authentication techniques: Overviews and open issues. *Bio-inspiring cyber security and cloud services: trends and innovations*, 423–446.

- Bansal, V., Garg, S., 2022. A cancelable biometric identification scheme based on bloom filter and format-preserving encryption. *Journal of King Saud University - Computer and Information Sciences* 34, 5810–5821. doi:[10.1016/j.jksuci.2022.01.014](https://doi.org/10.1016/j.jksuci.2022.01.014).
- Bok-Min, G., Abanda, Y., Tiedeu, A., Kom, G., 2021. Image encryption with fusion of two maps. *Security and Communication Networks* 2021, 6624890. URL: <https://doi.org/10.1155/2021/6624890>, doi:[10.1155/2021/6624890](https://doi.org/10.1155/2021/6624890).
- Cao, G., Yang, Y., Lei, J., Jin, C., Liu, Y., Song, M., 2017. Tripletgan: Training generative model with triplet loss. *CoRR* abs/1711.05084. URL: <http://arxiv.org/abs/1711.05084>, [arXiv:1711.05084](https://arxiv.org/abs/1711.05084).
- Deng, L., 2012. The mnist database of handwritten digit images for machine learning research. *IEEE Signal Processing Magazine* 29, 141–142.
- Dong, X., Shen, J., 2018. Triplet loss in siamese network for object tracking, in: Ferrari, V., Hebert, M., Sminchisescu, C., Weiss, Y. (Eds.), *Computer Vision – ECCV 2018*, Springer International Publishing, Cham. pp. 472–488.
- Galbally, J., Fierrez, J., Ortega-García, J., 2007. Vulnerabilities in biometric systems: Attacks and recent advances in liveness detection. *Database* 1, 1–8.
- Gatys, L.A., Ecker, A.S., Bethge, M., 2016. Image style transfer using convolutional neural networks, in: *2016 IEEE Conference on Computer Vision and Pattern Recognition (CVPR)*, pp. 2414–2423. doi:[10.1109/CVPR.2016.265](https://doi.org/10.1109/CVPR.2016.265).
- Goodfellow, I., Pouget-Abadie, J., Mirza, M., Xu, B., Warde-Farley, D., Ozair, S., Courville, A., Bengio, Y., 2014. Generative adversarial nets. *Advances in neural information processing systems* 27.
- Guo, D., Ge, S., Zhang, S., Gao, S., Tao, R., Wang, Y., 2022. Deepssn: A deep convolutional neural network to assess spatial scene similarity. *Transactions in GIS* 26. doi:[10.1111/tgis.12915](https://doi.org/10.1111/tgis.12915).

- Hamme, T.V., Garofalo, G., Joos, S., Preuveneers, D., Joosen, W., 2022. Ai for biometric authentication systems, in: Security and Artificial Intelligence: A Crossdisciplinary Approach. Springer, pp. 156–180.
- Helmy, M., El-Shafai, W., El-Rabaie, E.S.M., El-Dokany, I.M., El-Samie, F.E.A., 2022. A hybrid encryption framework based on rubik’s cube for cancelable biometric cyber security applications. Optik 258, 168773. doi:[10.1016/j.ijleo.2022.168773](https://doi.org/10.1016/j.ijleo.2022.168773).
- Hoffer, E., Ailon, N., 2015. Deep metric learning using triplet network, in: Similarity-Based Pattern Recognition: Third International Workshop, SIMBAD 2015, Copenhagen, Denmark, October 12-14, 2015. Proceedings 3, Springer. pp. 84–92.
- Huang, G.B., Ramesh, M., Berg, T., Learned-Miller, E., 2007. Labeled Faces in the Wild: A Database for Studying Face Recognition in Unconstrained Environments. Technical Report 07-49. University of Massachusetts, Amherst.
- Isola, P., Zhu, J., Zhou, T., Efros, A.A., 2016. Image-to-image translation with conditional adversarial networks. CoRR abs/1611.07004. URL: <http://arxiv.org/abs/1611.07004>, [arXiv:1611.07004](https://arxiv.org/abs/1611.07004).
- Kauba, C., Piciucco, E., Maiorana, E., Gomez-Barrero, M., Prommegger, B., Campisi, P., Uhl, A., 2022. Towards practical cancelable biometrics for finger vein recognition. Information Sciences 585, 395–417. doi:[10.1016/j.ins.2021.11.018](https://doi.org/10.1016/j.ins.2021.11.018).
- Kaur, H., Khanna, P., 2020. Privacy preserving remote multi-server biometric authentication using cancelable biometrics and secret sharing. Future Generation Computer Systems 102, 30–41. doi:[10.1016/j.future.2019.07.023](https://doi.org/10.1016/j.future.2019.07.023).
- Kausar, F., 2021. Iris based cancelable biometric cryptosystem for secure healthcare smart card. Egyptian Informatics Journal 22, 447–453. doi:[10.1016/j.eij.2021.01.004](https://doi.org/10.1016/j.eij.2021.01.004).
- Kingma, D.P., Ba, J., 2014. Adam: A method for stochastic optimization. arXiv preprint arXiv:1412.6980 .

- Kumar, S.K., 2017. On weight initialization in deep neural networks. CoRR abs/1704.08863. URL: <http://arxiv.org/abs/1704.08863>, [arXiv:1704.08863](https://arxiv.org/abs/1704.08863).
- Le, H.M., Samaras, D., 2019. Shadow removal via shadow image decomposition. CoRR abs/1908.08628. URL: <http://arxiv.org/abs/1908.08628>, [arXiv:1908.08628](https://arxiv.org/abs/1908.08628).
- Lee, M.J., Teoh, A.B.J., Uhl, A., Liang, S.N., Jin, Z., 2021. A tokenless cancellable scheme for multimodal biometric systems. *Computers & Security* 108, 102350. doi:[10.1016/j.cose.2021.102350](https://doi.org/10.1016/j.cose.2021.102350).
- Liu, Z., Yin, H., Wu, X., Wu, Z., Mi, Y., Wang, S., 2021. From shadow generation to shadow removal. CoRR abs/2103.12997. URL: <https://arxiv.org/abs/2103.12997>, [arXiv:2103.12997](https://arxiv.org/abs/2103.12997).
- Maćkiewicz, A., Ratajczak, W., 1993. Principal components analysis (pca). *Computers & Geosciences* 19, 303–342. URL: <https://www.sciencedirect.com/science/article/pii/009830049390090R>, doi:[https://doi.org/10.1016/0098-3004\(93\)90090-R](https://doi.org/10.1016/0098-3004(93)90090-R).
- Matoba, O., Nomura, T., Perez-Cabre, E., Millan, M.S., Javidi, B., 2009. Optical techniques for information security. *Proceedings of the IEEE* 97, 1128–1148. doi:[10.1109/JPROC.2009.2018367](https://doi.org/10.1109/JPROC.2009.2018367).
- Murakami, T., Ohki, T., Kaga, Y., Fujio, M., Takahashi, K., 2019. Cancellable indexing based on low-rank approximation of correlation-invariant random filtering for fast and secure biometric identification. *Pattern Recognition Letters* 126, 11–20. doi:[10.1016/j.patrec.2018.04.005](https://doi.org/10.1016/j.patrec.2018.04.005).
- Nayar, G.R., Thomas, T., Emmanuel, S., 2021. Graph based secure cancellable palm vein biometrics. *Journal of Information Security and Applications* 62, 102991. doi:[10.1016/j.jisa.2021.102991](https://doi.org/10.1016/j.jisa.2021.102991).
- Parkhi, O., Vedaldi, A., Zisserman, A., 2015. Deep face recognition, in: *BMVC 2015-Proceedings of the British Machine Vision Conference 2015*, British Machine Vision Association.
- Ronneberger, O., Fischer, P., Brox, T., 2015. U-net: Convolutional networks for biomedical image segmentation. CoRR abs/1505.04597. URL: <http://arxiv.org/abs/1505.04597>, [arXiv:1505.04597](https://arxiv.org/abs/1505.04597).

- Schroff, F., Kalenichenko, D., Philbin, J., 2015. Facenet: A unified embedding for face recognition and clustering. CoRR abs/1503.03832. URL: <http://arxiv.org/abs/1503.03832>, [arXiv:1503.03832](https://arxiv.org/abs/1503.03832).
- Spruyt, V., 2018. Loc2vec: Learning location embeddings with triplet-loss networks. Sentiance web article: <https://www.sentiance.com/2018/05/03/venue-mapping>.
- Subramanian, N., Elharrouss, O., Al-Maadeed, S., Bouridane, A., 2021. Image steganography: A review of the recent advances. IEEE Access 9, 23409–23423. doi:[10.1109/ACCESS.2021.3053998](https://doi.org/10.1109/ACCESS.2021.3053998).
- Vasluianu, F.A., Romero, A., Van Gool, L., Timofte, R., 2021. Shadow removal with paired and unpaired learning, in: 2021 IEEE/CVF Conference on Computer Vision and Pattern Recognition Workshops (CVPRW), pp. 826–835. doi:[10.1109/CVPRW53098.2021.00092](https://doi.org/10.1109/CVPRW53098.2021.00092).
- Wang, F., Xiang, X., Cheng, J., Yuille, A.L., 2017a. Normface: L_2 hypersphere embedding for face verification. CoRR abs/1704.06369. URL: <http://arxiv.org/abs/1704.06369>, [arXiv:1704.06369](https://arxiv.org/abs/1704.06369).
- Wang, S., Deng, G., Hu, J., 2017b. A partial hadamard transform approach to the design of cancelable fingerprint templates containing binary biometric representations. Pattern Recognition 61, 447–458. doi:[10.1016/j.patcog.2016.08.017](https://doi.org/10.1016/j.patcog.2016.08.017).
- Yang, P., Zhang, M., Wu, R., Su, Y., Guo, K., 2022a. Hiding image within image based on deep learning. Journal of Physics: Conference Series 2337, 012009. URL: <https://dx.doi.org/10.1088/1742-6596/2337/1/012009>, doi:[10.1088/1742-6596/2337/1/012009](https://doi.org/10.1088/1742-6596/2337/1/012009).
- Yang, W., Wang, S., Hu, J., Zheng, G., Valli, C., 2018. A fingerprint and finger-vein based cancelable multi-biometric system. Pattern Recognition 78, 242–251. doi:[10.1016/j.patcog.2018.01.026](https://doi.org/10.1016/j.patcog.2018.01.026).
- Yang, W., Wang, S., Kang, J.J., Johnstone, M.N., Bedari, A., 2022b. A linear convolution-based cancelable fingerprint biometric authentication system. Computers & Security 114, 102583. doi:[10.1016/j.cose.2021.102583](https://doi.org/10.1016/j.cose.2021.102583).

- Yang, W., Wang, S., Shahzad, M., Zhou, W., 2021. A cancelable biometric authentication system based on feature-adaptive random projection. *Journal of Information Security and Applications* 58, 102704. doi:[10.1016/j.jisa.2020.102704](https://doi.org/10.1016/j.jisa.2020.102704).
- Zhang, S., Zhang, Q., Wei, X., Zhang, Y., Xia, Y., 2018. Person re-identification with triplet focal loss. *IEEE Access* 6, 78092–78099. doi:[10.1109/ACCESS.2018.2884743](https://doi.org/10.1109/ACCESS.2018.2884743).
- Zhang, Y., Zhang, L.Y., Zhou, J., Liu, L., Chen, F., He, X., 2016. A review of compressive sensing in information security field. *IEEE Access* 4, 2507–2519. doi:[10.1109/ACCESS.2016.2569421](https://doi.org/10.1109/ACCESS.2016.2569421).
- Zhao, H., Gallo, O., Frosio, I., Kautz, J., 2017. Loss functions for image restoration with neural networks. *IEEE Transactions on Computational Imaging* 3, 47–57. doi:[10.1109/TCI.2016.2644865](https://doi.org/10.1109/TCI.2016.2644865).
- Zhmoginov, A., Sandler, M., 2016. Inverting face embeddings with convolutional neural networks. ArXiv abs/1606.04189. URL: <https://api.semanticscholar.org/CorpusID:15785666>.